J. theor. Biol. (2001) **212,** 275–294
doi:10.1006/jtbi.2001.2375, available online at http://www.idealibrary.com on IDEAL®

Light-triggered pH Banding Profile in *Chara* Cells Revealed with a Scanning pH Microprobe and its Relation to Self-Organization Phenomena

A. A. Bulychev*, A. A. Polezhaev†, S. V. Zykov‡§, T. Yu. Pljusnina*, G. Yu. Riznichenko*, A. B. Rubin*, W. Jantoß§, V. S. Zykov§‖ and S. C. Müller§

**Faculty of Biology, Moscow State University*, 119899 *Moscow, Russia, †P. N. Lebedev Physical Institute*, 117924 *Moscow, Russia, ‡Faculty of Physics, Moscow State University*, 119899 *Moscow, Russia and §Institut für Experimentelle Physik, Otto-von-Guericke-Universität, D*-39106 *Magdeburg, Germany*

(*Received on* 8 *December* 2000, *Accepted in revised form on* 14 *June* 2001)

When exposed to light, Characean cells develop a pattern of alternating alkaline and acid bands along the cell length. The bands were identified with a tip-sensitive antimony pH microelectrode positioned near one end of *Chara* internode at a distance of 50–100 μm from the cell wall. The stage with *Chara* cell was moved along its longitudinal axis at a computer-controlled speed (100 or 200 $\mu m\,s^{-1}$) relative to the pH probe over a distance of 50 mm. Under sufficient uniform illumination of the cell (from 100 to 2.5 $W\,m^{-2}$), the homogeneous pH distribution becomes unstable and a banding pattern is formed, the spatial scale of which decreases with the light intensity. If the cell is locally illuminated, bands are formed only in the region of illumination. It is shown that the inhibition of cyclosis by cytochalasin B leads to the disappearance of the banding pattern. The addition of ammonium (weak base) inhibited the banding pattern, whereas acetate (weak acid) alleviated the inhibitory effect of ammonium and restored the pH banding. A model explaining the observed phenomena is formulated in terms of proton concentration outside and bicarbonate concentration inside the cell. It contains two diffusion equations for the corresponding ions with nonlinear boundary conditions determined by ion transport processes across the cell membrane. The model qualitatively explains most of the experimental observations. It describes the dependence of the pattern characteristics on the light intensity and reveals the role of cyclosis in this phenomenon.

Introduction

Investigating the principles of spatio-temporal self-organization in living systems is a major challenge for theoretical biology (Murray, 1989). Much of the research in modern biology, both experimental and theoretical, is devoted to determining the underlying mechanisms which generate heterogeneous spatial patterns from an initially uniform state. A theory based on a reaction–diffusion mechanism was put forward in the classical paper by Turing (1952). The general idea of this theory is that under certain conditions a uniform distribution of chemicals which can react and diffuse, can become unstable, and a steady spatial pattern emerges.

Examples of self-organization can be found on the level of communities of uni-cellular organisms as well as in a single multi-cellular organism

‖Author to whom correspondence should be addressed.
E-mail: vladimir.zykov@physik.uni-magdeburg.de

0022–5193/01/190275 + 20 $35.00/0

(for an overview see, for instance, Müller & Plesser, 1992). Usually, complex re-arrangements of the spatial cell distribution take place, which are influenced by chemical and mechanical interactions between cells. This is impressively documented in growing bacterial colonies (Budrene & Berg, 1991) or in aggregating amoebae of the slime mould *Dictyostelium discoideum* (Devreotes, 1989; Siegert & Weijer, 1993). Another example of self-organization phenomena is the appearance of a spatial pattern in a single cell frequently considered as a basis for morphogenesis (Jaffe, 1977). In many cases, the observed spatio-temporal patterns can be explained as a result of a Turing instability (Turing, 1952) [e.g. some morphogenetic processes (Meinhardt, 1982; Murray, 1989; Kondo & Asai, 1995)].

A remarkable example of self-organization phenomena are banding structures formed by Characean cells (Toko *et al*., 1985). When exposed to light, internodal cells of *Chara* and *Nitella* develop a pattern of alternating acid and alkaline bands along the cell length (Spear *et al*., 1969; Lucas, 1982, 1983; Ogata, 1983; Smith & Walker, 1983; Coster *et al*., 1985; Toko *et al*., 1988; Fisahn & Lucas, 1992). This pattern has a characteristic length scale of 3–10 mm. The pH pattern in young cells has no correlation with any visible morphological structures, whereas older cells show permanent precipitates of $CaCO_3$ in the alkaline zones (Arens, 1939). The formation of the pH pattern along *Chara* cells is related to the ATP-dependent H^+-extruding proton pump of the plasmalemma, while the proton sinks are located in alkaline zones (Walker *et al*., 1979; Toko *et al*., 1985, 1988). According to Walker & Smith (1977) this process is associated with the appearance of an electrochemical gradient which induces circulating electric currents between acid and alkaline regions. Neither the mechanism nor the functional significance of the pH bands have been elucidated yet with certainty. There are speculations that the banding patterns in Characean cells show similarity with the formation of circulating currents in elongating roots (Iwabuchi *et al*., 1989; Toko *et al*., 1987b) and with transleaf pH gradients in some aquatic plants (Elzenga & Prins, 1989). Metraux and coworkers (1980) assume that this segmentation process provides the basis for a cellular elongation mechanism that is limited to the acid regions. Another hypothesis concerning the physiological role of banding patterns in Characean cells is that alternating regions of high and low electric potential cause loops of electric current that extend outward from the cell into the outer medium, thereby providing a mechanism for electrophoretic transport in the layer near the membrane (Dorn & Weiseneel, 1984). Such a mechanism could increase the supply of HCO_3^- for the internodal cells in their stagnant water habitat.

An internodal Characean cell has the form of a cylinder with a diameter of 0.6–1.0 mm and a length of 40–80 mm (see Fig. 1). The major part of the cell volume is occupied by the central vacuole. In a thin layer between the plasmalemma and the vacuole, one observes a flow of cytoplasm in the longitudinal direction (cyclosis). Various ions are transported both into and out of the cells across the membrane. Among the ion fluxes which may determine the banding patterns of pH and current profiles are those of bicarbonate (HCO_3^-), hydroxyl (OH^-) and proton (H^+) (Lucas, 1976, 1979; Lucas & Nuccitelli, 1980).

Up to now, the alternating acid and alkaline domains have mostly been detected with the vibrating probe as a sensor of inward and outward transmembrane currents near the cell surface (Fisahn & Lucas, 1992). However, vigorous mixing caused by the vibrating probe perturbs the diffusion gradients. Moreover, the requirement of low and uniform conductance of the experimental solution restricts the application of this approach. Early attempts to measure the longitudinal pH profiles were based on point-by-point measurements and offered only low spatial and temporal resolution. Thus, more refined techniques are required. In previous work, antimony

FIG. 1. Stationary distribution of alkaline and acid regions around an illuminated *Chara* cell. The pattern was visualized using phenol red at a concentration of 25 μM. Dark spots correspond to alkaline regions.

pH microelectrodes were applied as a useful approach for studying proton transport in the unstirred layers near the bimolecular lipid membranes (Antonenko & Bulychev, 1991). This type of electrode is a fast-responding pH sensor with a linear relationship between electrode potential and pH.

Several mechanisms for the explanation of the banding phenomenon in Characean cells have been suggested. In one of them ion pumps or channels are assumed to re-organize on the cell membrane electrophoretically due to the electric field created by the pumps themselves (Jaffe *et al*., 1974; Larter & Ortoleva, 1982; Fromherz, 1988a, b; Polezhaev & Saburov, 1991). Although this mechanism is in principle possible, its characteristic time appears to be of the order of 10^8 s, much too long compared with the typical scale of hours or even minutes observed in experiments. Toko and co-workers (1985, 1987a) developed a model in which the proton pumps, uniformly distributed along the plasma membrane, influence the proton distribution inside and outside the cell. The steady state of the uniform membrane potential may become unstable, but under the unrealistic hypothesis that the proton efflux rises with the increase of the external proton concentration. Leonetti & Pelce (1994) suggested a mechanism for the banding patterns based on H^+/HCO_3^- symport. According to their model an instability is possible only for a stoichiometry factor $n > 1$, which is in conflict with the experimental finding that the H^+/HCO_3^- symport is electrically neutral ($n = 1$) (Lucas, 1983). Thus, the existing theoretical approaches to the explanation of patterns in Characean cells need further improvement.

In this paper, we present experimental data on banding pattern formation in *Chara* cells and especially on the role of light in this phenomenon. We also give a theoretical interpretation of these observations. In the first section, we describe the elaboration of a scanning technique for studying periodical structures in longitudinal pH profiles along *Chara* cells. In the second section, we present the results obtained with the help of this technique. Then, we formulate a phenomenological model, which qualitatively explains the experimental observations, present results of the numerical simulations of the model and compare them with the experimental data. Finally, we discuss the possible development of the study.

Materials and Methods

PLANT MATERIAL AND SOLUTIONS

Chara corallina Klein ex Willd. was grown in 20-l glass vessels under scattered daylight at room temperature (20–22°C). We used cells without apparent signs of calcification. Single internodes measuring 6–7 cm in length and about 1 mm in diameter were cut from the plant and placed in APW (artificial pond water) containing 0.1 mM KCl, 1.0 mM NaCl, and 0.1 mM $CaCl_2$. This medium was employed in most experiments. Solutions containing phenol red, cytochalasin B, and fusicoccin were prepared from 5, 3 and 1.33 mM stock solutions, respectively. All chemicals were analytical grade, purchased from Sigma (USA) and Serva (Germany).

EXPERIMENTAL SET-UP

Prior to an experiment, the cell was placed in a transparent Plexiglas chamber, which was mounted on a movable table controlled by a C-804 DC-Motor Controller (Physik Instrumente, Waldbronn, Germany). The mechanical stage of this device ensures linear resolution of about 0.1 $\mu m\, s^{-1}$ and provides a two-coordinate movement of cell. Two chambers of different geometry were used. One chamber with a volume of 2.5 ml had a long 6-mm-wide slit where the cell was aligned with small Plexiglas spacers. This chamber was convenient to use, but because of its small volume, the pH of the external medium increased during illumination, which violated the stationarity of experimental conditions. Another chamber with dimensions of $100 \times 100 \times 5$ mm (total volume 50 ml) was employed to eliminate geometry-related restrictions for the diffusion of components transferred across the plasmalemma. While the bulk pH in this chamber remained practically constant under illumination, the disadvantage of this chamber is that the experiment should be preferably performed in a gel in order to avoid hydrodynamic flows. The cell under study was positioned in the centre of either chamber. Experiments were conducted at room temperature. Illumination of the chamber was

provided with a slide projector via a light-reflecting mirror. The maximum irradiance at the solution surface was $100\,W\,m^{-2}$. Cells were illuminated from underneath through the transparent bottom of the experimental chamber and observed from the top with a microscope.

pH SCANNING MEASUREMENTS

Alkaline and acid bands were identified with pH microelectrodes. Tip-sensitive antimony pH microelectrodes were prepared as previously described (Remis *et al.*, 1986). First, melted antimony was sucked into Pyrex glass capillaries (1.2 mm outer diameter). Next, microelectrodes were pulled on a vertical microelectrode puller. Microelectrodes with a tip diameter ranging between 20 and 50 $\mu m\,s^{-1}$ were used. The potential difference between the pH probe and a Ag/AgCl reference electrode was calibrated as a function of pH using standard buffer solutions. The slope of the electrode characteristic was 58 ± 1 mV (pH unit)$^{-1}$. The potential difference was measured with a high-impedance electrometric amplifier (VAJ-51, Germany), digitized at a frequency of 5 Hz, and recorded on a computer. The pH microelectrode was mounted in an electrode holder and positioned with a micromanipulator near one end of *Chara* internode at a distance of 50–100 μm from the cell wall. The onset of motor movement was synchronized with the beginning of data acquisition. The chamber with *Chara* cell moved along its longitudinal axis at a controlled speed (mostly 100 or 200 $\mu m\,s^{-1}$). The movement of the pH electrode relative to the cell was observed with a microscope equipped with a CCD camera. Preliminary experiments showed that a velocity of 100 $\mu m\,s^{-1}$ ensures the recording of pH bands without significant attenuation, whereas high-speed recording (400 $\mu m\,s^{-1}$) attenuates the amplitude of bands by about 25%. The initial and target positions on the cell were programmed in the beginning of each experiment and were the same in all consecutive measurements, covering a distance of usually 50 mm. The computer-controlled movable stage ensured accurate and reproducible displacements of *Chara* internode with an accuracy of $1\,\mu m\,s^{-1}$. The recording of an individual pH profile took 4–7 min.

Results

pH PATTERNS UNDER HOMOGENOUS AND STATIONARY ILLUMINATION

Longitudinal pH Profiles

Under homogeneous stationary white light the alkaline and acid global banding pattern in *Chara* cell was visualized by (25 μM) phenol red. At acid pH, the main absorption band of phenol red is around 430 nm (yellow solution), at alkaline pH it is around 559 nm (red or purple solution). Figure 1 shows the stationary distribution of pH around the cell. The dark spots in the figure correspond to alkaline bands.

Figure 2(a) exemplifies the longitudinal pH profile in *Chara* cell. Five to seven alkaline bands were often observed at a cell length of 50 mm, but substantial variations in this number were noted. Some cells showed more frequent bands, and, in the other extreme, only one acid and one alkaline bands are located at the opposite ends of *Chara* internode. The difference in pH between alkaline and acid zones reaches 2–3 pH units. The banding pattern, i.e. the position of bands and their amplitudes, was fairly well reproduced in sequential measurements. The bands did not migrate under steady-state conditions. After full refreshment of the medium in the bath, the banding profile (at a distance of about 100 μm from the cell) could be recorded almost unattenuated in magnitude already after 3 min.

Simultaneous measurements of pH traces and video records of alternating white (acid) and dark (alkaline) zones showed a strong correlation between the pH-electrode signal and the staining of the bath in the vicinity of a cell (results not shown).

Transversal pH Profiles in Acid and Alkaline Zones

Figure 2(b) shows the radial profiles of pH in alkaline and acid zones that were measured during the controlled withdrawal of pH probe from the cell surface. These measurements were performed in a large-volume chamber in order to avoid restrictions for diffusion of ions and solutes transported across the plasmalemma. Under these experimental conditions, the external volume can be considered infinite. In the case of a small-volume chamber, the pH in the bulk

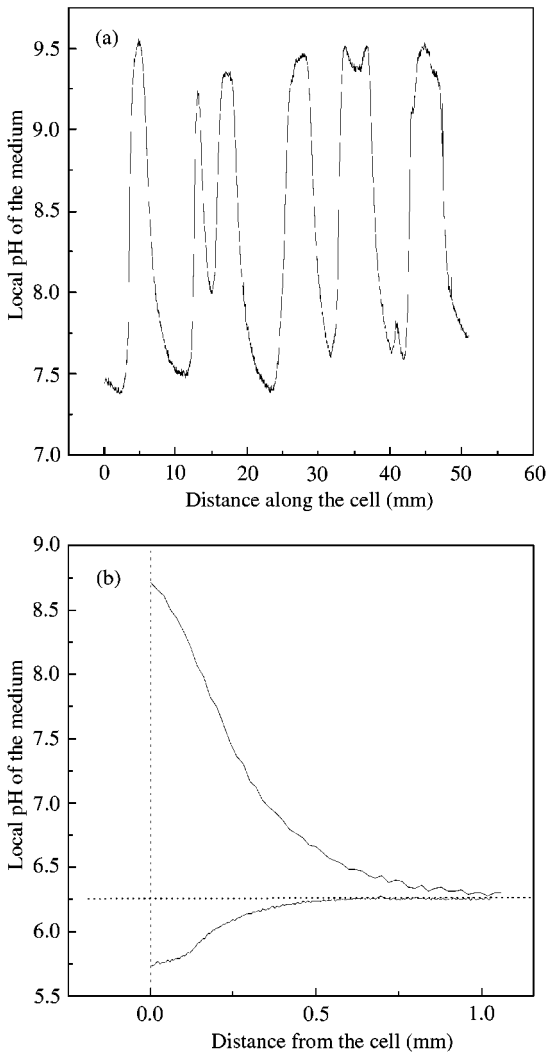

FIG. 2. Stationary distribution of pH near an illuminated *Chara* cell. (a) Longitudinal profile of pH in the external medium near the surface of a *Chara* cell, obtained by scanning with a pH microelectrode at a velocity of 200 $\mu m\,s^{-1}$. The cell was placed in the narrow-slit chamber filled with APW and illuminated with white light at an intensity of 100 $W\,m^{-2}$. (b) Transversal profiles of external pH in the alkaline (1) and acid (2) zones near illuminated *Chara* cell. The cell was placed in the large-volume chamber (50 ml total volume) to exclude geometric factor. The pH microelectrode was withdrawn from the cell surface in the direction normal to the membrane at a velocity of 20 $\mu m\,s^{-1}$. Other conditions as in Fig. 1(a). The dotted lines show the pH in the bulk phase and the initial position of the electrode touching the cell wall, respectively.

phase increased during illumination owing to photosynthetic fixation of CO_2, whereas in the large-volume chamber the pH remained virtually at a constant level. As can be seen from Fig. 2(b), pH in the alkaline zone near the cell surface is substantially higher than in the bulk phase, and the pH in the acid region near the surface is lower than in the bulk phase. These opposite pH shifts present strong evidence against the possible alternative that local pH values both in alkaline and acid regions are higher than the bulk pH, although to a different extent.

When the pH microelectrode was positioned near the cell in the alkaline or acid region, small fluctuations of pH (of about 0.02 pH unit) were observed. The period of fluctuations was 2–4 min, for both acid and alkaline zones, with slightly longer periods for acidic regions. These temporal fluctuations are interesting in that they may reflect intrinsic properties of membrane transport systems (Lucas & Nuccitelli, 1980). Certainly, small fluctuations in the distance between the cell and the electrode could also cause these pH fluctuations, because the plot of pH against this distance is rather steep [see Fig. 2(b)]. Since the amplitude of fluctuations is at least two orders of magnitude smaller than the pH shifts between acid and alkaline zones, we consider pH profiles as stationary structures.

Unclosed Bands

We noticed that, in some *Chara* cells, scanning with pH microelectrode along different sides of a cylindrical internode yielded different pH profiles. This phenomenon is illustrated in Fig 3. In these experiments, the electrode moved relative to the cell along three different pathways (see inset in Fig. 3). The electrode was placed either above the cell (path 1) or on its opposite lateral sides (paths 2 and 3). Five alkaline bands were recorded in the pH profile along path 3. The profiles were fairly well reproduced during the experiment, as shown by three curves assigned to this pathway. However, the profiles measured upon scanning along pathways 1 and 2 missed some alkaline bands. These profiles contained one small band, the position of which was common for all three pathways (band 2 of the path-3 profile), whereas other bands in path-1 and path-2 profiles had different positions coinciding with either band 4 or 5 of the path-3 profile. All these profiles were reproduced in serial measurements.

These observations provide evidence that alkaline regions in some *Chara* cells have no radial

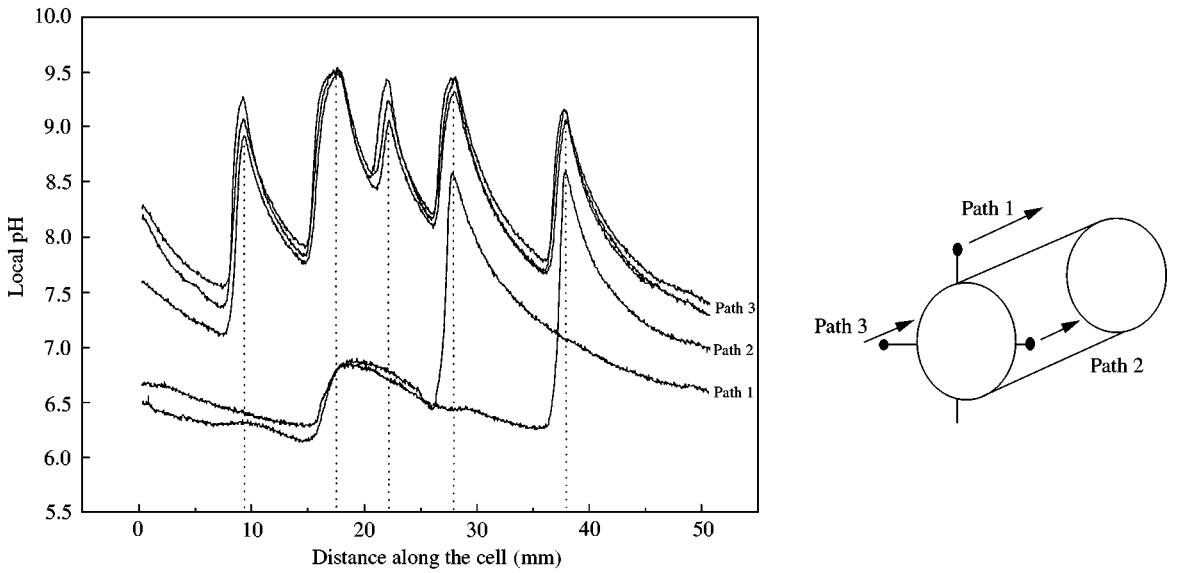

FIG. 3. Demonstration of unclosed bands or disk-shaped stripes. The pH profiles were obtained by scanning with the pH microprobe along different pathways as schematically shown on the right side of the figure. For path 3, three measurements are presented to demonstrate the reproducibility of the profiles.

symmetry: they represent either large spots or unclosed rings. That is why the profiles measured along different pathways are characterized by some common and some missing peaks, as shown in Fig 3.

In the cells showing unclosed bands, non-monotonous transversal pH profiles were observed. In these experiments, the longitudinal coordinate of the pH probe was first fixed near the alkaline spot. Then, the electrode was slightly re-adjusted in vertical and horizontal directions so that its position near the cell did not exactly match the alkaline spot. Upon withdrawing the electrode from the cell, the pH changed non-monotonously, reaching a maximum and decreasing to a bulk level. Apparently, during its movement, the electrode crossed the region of high pH, related to OH^- diffusion from alkalizing membrane-transport domains. When the pH electrode was withdrawn from the boundary to the bulk solution starting from the centre of alkaline spot, the transversal pH profiles displayed no transitory peak.

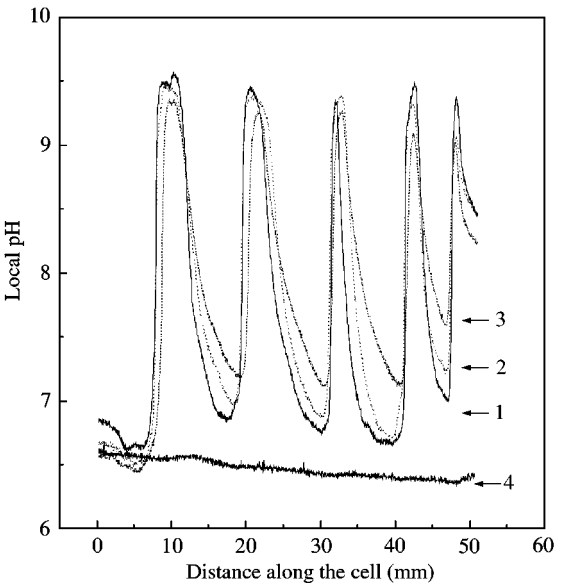

FIG. 4. Band pH profiles measured at different light intensities: 1–100 $W\,m^{-2}$, 2–5 $W\,m^{-2}$, 3–2.5 $W\,m^{-2}$, 4–250 $mW\,m^{-2}$. Measurements were started at high and continued at progressively lower light intensities. At each intensity, the cell was adapted for at least 30 min, while pH profiles were regularly measured every 10–15 min.

LIGHT-CONTROLLED PATTERNS

Effect of Light Intensity

The sustained pH pattern was only observed under illumination with sufficiently high intensity, which is in line with previous findings (Lucas & Nuccitelli, 1980; Toko *et al.*, 1985). Transformation of the band structures under the reduction of the light intensity from 100 to 2.5 $W\,m^{-2}$ is shown in Fig. 4. Each profile was recorded

at least 30 min after the reduction of light intensity, when the steady-state conditions were presumably achieved. The attainment of the steady state was tested by repetitive measurement of pH profiles. For example, after the reduction of light intensity from 5 to 2.5 $W m^{-2}$, the pH profile was measured every 15 min for a period of 1.5 hr; only minor changes in the pH profile were noted in the last hour. As is seen from Fig. 4, at light intensity of 2.5 $W m^{-2}$, the amplitude of pH peaks was reduced by only 20% with respect to their extent at full light (100 $W m^{-2}$). However, further reduction in light intensity to 0.25 $W m^{-2}$ resulted in the complete inhibition of pH pattern.

The transition to a homogeneous pH distribution along the cell after the exposure to low light (0.25 $W m^{-2}$) proceeded via the reduction in the number of bands and non-uniform attenuation of different bands. These characteristic changes were in striking contrast to a conceivable possibility of the proportional reduction of all the bands until complete flattening of the profile.

The results indicate the existence of a threshold light intensity, rather than a gradual increase of pH peaks with light intensity. When the banding pattern was suppressed by insufficient light, the re-exposure to a light intensity of 2.5 $W m^{-2}$ did not lead to the restoration of banding pattern within at least 1 hr. Higher light intensities were required to restore the pH banding profile, which suggests the presence of a hysteresis in the appearance and disappearance of pH banding, consistent with earlier observations.

Dynamics of Band Formation

Since the dynamics of band formation may yield insight into their origin, we monitored the restoration of pH profiles along the cell length after the re-exposure of a dark-adapted cell to bright light (Fig. 5). As can be seen from Figs 5(a) and (b), the pH banding profile completely disappeared after a 90-min adaptation of the cell in darkness. After the subsequent re-exposure of the cell to bright light (100 $W m^{-2}$), the pH near the cell surface started to increase, presumably owing to the photosynthetic fixation of CO_2 [cf. Figs 5(b) and (c)]. This increase was accompanied by the appearance of irregular pH fluctuations in the longitudinal profile [Fig. 5(c)]. At a later stage, the amplitude of pH fluctuations continued to increase, and after a 20-min illumination, the formation of alkaline and acid bands was almost accomplished [Fig. 5(d), solid line]. The position of the main bands coincided with the position of the initial bands, but the new profile contained additional bands not present in the initial state. This feature is clearly seen in Fig. 5(d), where the newly formed banding pattern (solid curve) is superimposed on the initial pattern (dotted curve). The supplementary pH peaks disappeared gradually during prolonged illumination. For example, the profile shown in Fig. 5(e), differs from that shown in Fig. 5(d) by the lack of one supplementary peak.

Non-homogeneous Illumination of the Cell

We investigated modifications in the banding pattern under partial and local illumination of the cell, as well as after transition from local to overall illumination. When one-half of the cell was placed in darkness, the bands disappeared in the darkened part but not in the illuminated part of a cell (data not shown). The effect was reversible: bands re-appeared when the whole cell was exposed to light.

Figure 6 shows an experiment, in which the central (4 mm wide) part of the cell was exposed to light, whereas the remaining parts were kept in darkness. Under these conditions, two closely positioned alkaline bands were formed on the edges of the illuminated zone [Fig. 6(a)]. Following the transition from local to overall illumination, new bands appeared rather fast after a lag period of 5–10 min [Figs 6(b) and (c)]. The bands appeared one by one, which is in contrast to the conceivable possibility of gradual and simultaneous increase of all bands. Eventually, one of two closely opposed bands disappeared in the central part of the cell. Apparently, the distance between the bands in the doublet was not compatible with the larger periodic length characteristic for the cell under overall illumination [Fig. 6(d)].

INFLUENCE OF CHEMICAL AGENTS ON pH BANDING

In addition to light, other factors may exert a control over pattern-forming mechanisms. To

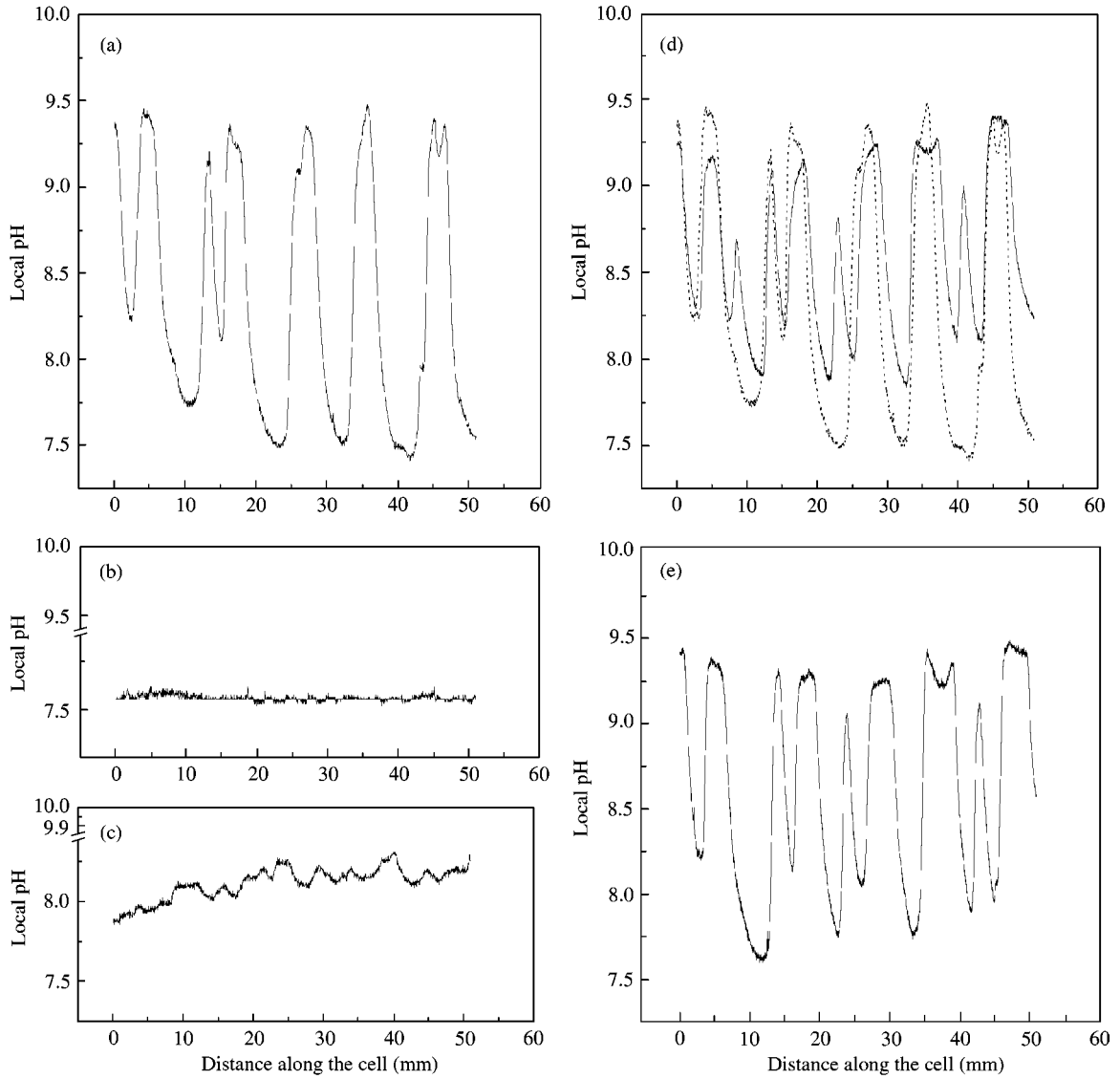

FIG. 5. Formation of banding patterns upon illumination of a dark-adapted *Chara* cell: (a) initial pH profile under stationary illumination; (b) suppression of banding after 100 min in darkness; (c) appearance of pH fluctuations after 5 min in light; (d) pH pattern with pronounced bands— 20 min in light; (e) disappearance of one pronounced band—50 min in light. The initial pH profile (dotted line) is shown for comparison in (d).

get information about such factors we applied several chemical treatments.

Effect of Potassium Chloride

Potassium ions are known to depolarize the plasmalemma. Thus, KCl can be used as an indirect tool to assess the role of the electric membrane potential. Although KCl increases the conductivity of the external medium, this conductivity should not be a limiting factor for circulating local currents, because of much lower membrane conductance. The replacement of artificial pond water (APW) with the solution containing 10 mM KCl brings about gradual suppression of all the bands. This suppression was still incomplete after 30 min incubation but, after longer exposure, only small peaks were observed in the pH profile. This result points to the possible role of cell membrane potential in the generation of pH patterns.

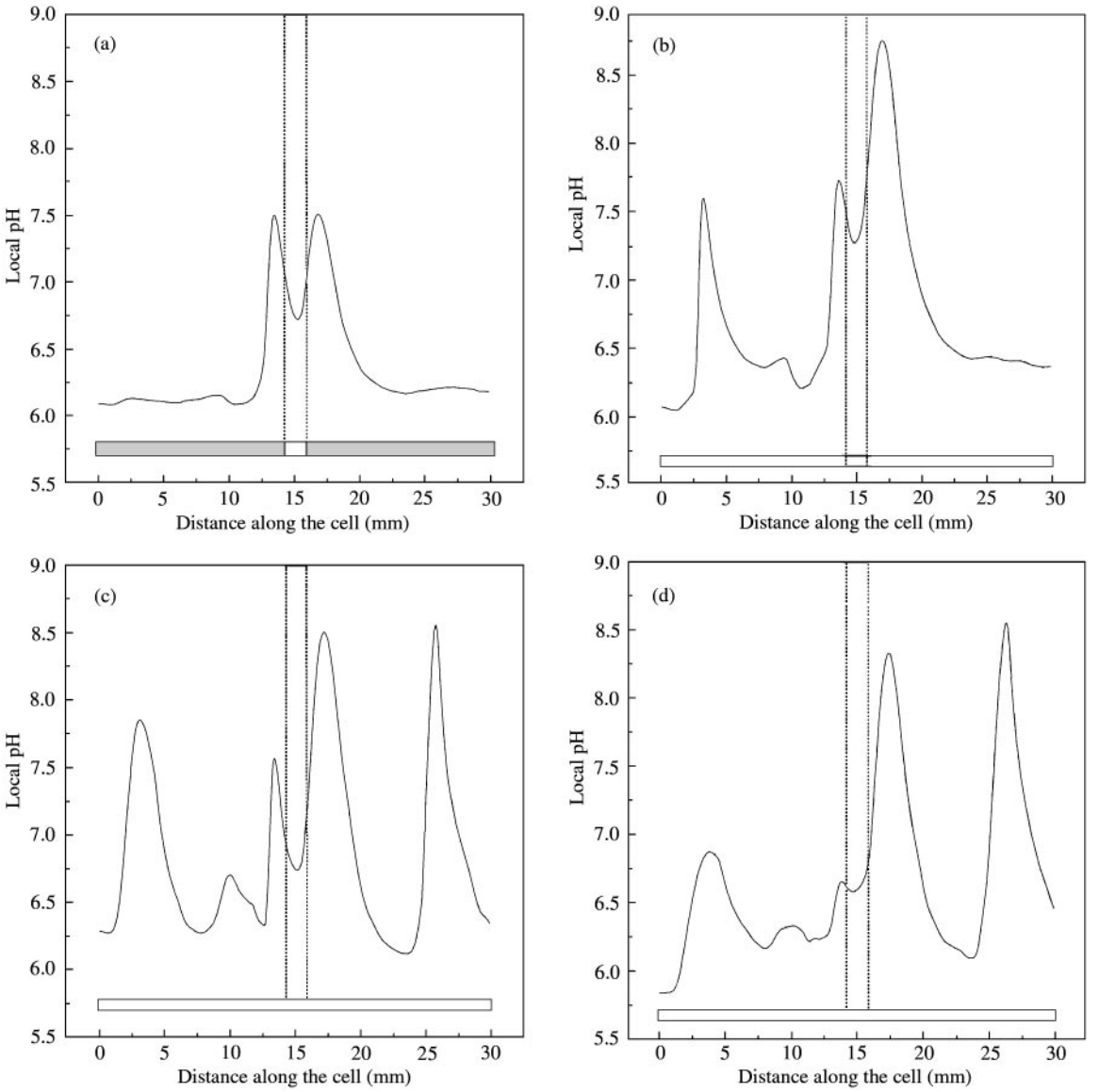

FIG. 6. pH pattern induced by local illumination of the central region of *Chara* internode and evolution of banding pattern after transition from local to overall illumination. (a) Two closely positioned bands form at the borders of the illuminated zone; the bar under the curve indicates the cell fragment with illuminated (width 4 mm) and darkened regions; (b)–(d) Banding profiles measured at different times after transition from local to overall illumination: (b) 12 min (c) 25 min and (d) 50 min. New bands appear sequentially. One of two initial bands in the doublet is eventually eliminated.

Weak Bases and Acids

The transmembrane proton transport directed outward and inward in acid and alkaline zones, respectively, should be sensitive to changes in cytoplasmic pH. The experimental approach to modify the cytoplasmic pH is based on the ability of weak bases and weak acids to penetrate through the membrane in the neutral form and affect the acid–base equilibrium in the cytoplasm. For example, when NH_4^+ in equilibrium with NH_3 ($NH_4^+ = NH_3 + H^+$) is present in the outer medium, the neutral form penetrates into the cytoplasm and binds protons, thereby giving rise to alkalization of the cytoplasm and the respective acidification of the boundary water layers in the outer medium (Smith, 1980; Antonenko & Bulychev, 1991).

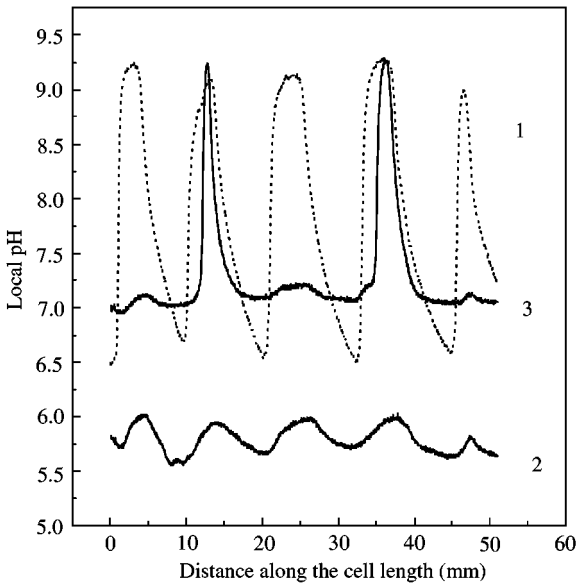

FIG. 7. Elimination of banding pattern by 10 mM NH_4Cl and its restoration after washing the cell with 10 mM acetate. The pH profiles were first measured in APW (curve 1). Then, 10 mM NH_4Cl (dissolved in APW) was applied to the bath medium for 7 min and washed out (curve 2). After removal of NH_4Cl, the bands were not restored within 30 min. Next, 10 mM sodium acetate was applied for 30 min and, when the alkaline peak appeared, acetate was washed out (curve 3).

In our experiments, the replacement of APW with APW containing 10 mM NH_4Cl resulted in a rapid suppression of the banding pattern (Fig. 7). The unstirred layers of medium near the cell were acidified, as predicted. The cytoplasmic streaming did not cease under this treatment. In addition to its effect on cytoplasmic pH, ammonium may affect the membrane potential similarly to K^+ ions, because the plasmalemma of Characean algae reportedly contains the uniport system for NH_4^+ (Walker *et al.*, 1979). Although the depolarizing effect of ammonium may be similar to that of K^+, the suppression of the banding pattern by ammonium was stronger (Fig. 7, curve 2) and developed within a few minutes, rather than tens of minutes. The removal of NH_4Cl from the medium did not lead to the restoration of bands, at least within 30 min.

As shown by curve 3 in Fig. 7, a partial recovery of pH banding was achieved after washing the cell with 10 mM sodium acetate. Acetate, a weak acid anion, easily penetrates through the membranes in undissociated form (CH_3COOH) and dissociates in the cytoplasm releasing protons, which gives rise to acidification of the cytoplasm and the respective alkalization of the outer medium near the membrane (Reid *et al.*, 1989; Antonenko & Bulychev, 1991). At a concentration of 1 mM, acetate stimulated band formation in the absence of ammonium. The observed inhibition of pH banding by NH_4^+ and the release of inhibition by acetate suggest that slight acidification of the cytoplasm is favourable for pH banding, whereas alkalization of cytoplasm inactivates the band-forming mechanisms.

Fusicoccin and Cytochalasin B

The plasmalemma proton pump is known to be activated by fusicoccin (Marre, 1979). In our experiments, the addition of fusicoccin at concentrations ranging from 2 to 10 μM led to a substantial acidification of the boundary layers in the external medium and increased the peak amplitudes in the pH profiles. This confirms the stimulating effect of fusicoccin on the plasmalemma H^+ pump and substantiates the role of the proton pump in the band-forming mechanism.

There have been reports that the inhibition of cyclosis transforms the band pattern to numerous small disc-shape patterns (cited after Toko *et al.*, 1985). In our work, the addition of cytochalasin B to the medium at a concentration of 40 μM inhibited cyclosis and caused the banding pattern to disappear (Fig. 8). Apparently, the cytoplasmic streaming is significant for the operation of band-forming mechanisms.

The Model

In this section, a phenomenological mathematical model for the banding phenomenon in a *Chara* cell is presented, which shows the pH bands along the cell length to be a self-organized pattern and qualitatively explains the results obtained experimentally.

The observed pH profiles are obviously the consequence of the ion transport processes across the cell membrane. According to Lucas & Nuccitelli (1980), the fluxes associated with HCO_3^- and OH^- transport are much larger in *Chara* cells than in any other of the presently known

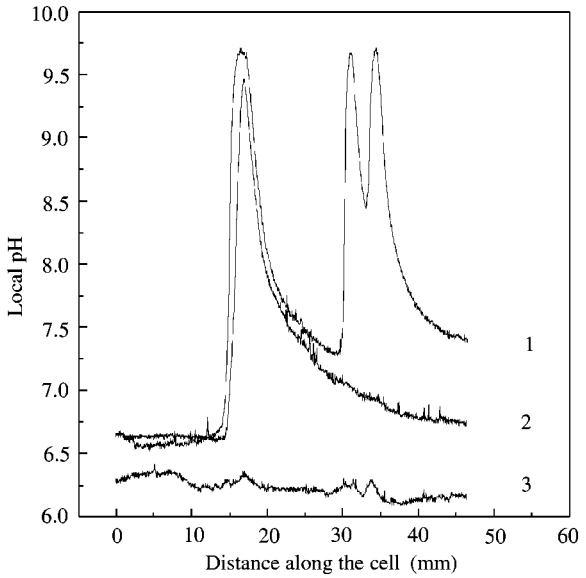

FIG. 8. Effect of cytochalasin B, an inhibitor of cytoplasmic streaming on pH banding pattern: 1—untreated cell; 2—cell 10 min after the addition of 45 μM cytochalasin B; 3—20 min after addition of cytochalasin.

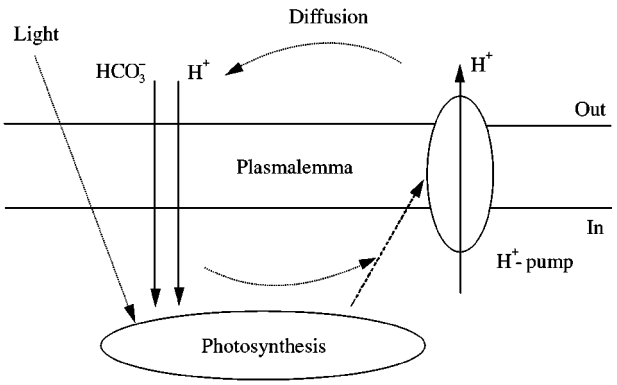

FIG. 9. Schematic representation of the processes in the membrane of the *Chara* cell considered relevant to the formation of band pattern.

ionic fluxes. However, as the proton concentration is strictly bounded to the concentration of the OH^- ions through the dissociation constant of water, it is clear that OH^- efflux described in experiments may be interpreted as H^+ influx. There exists an active H^+ efflux due to ATP-consuming H^+ pumps and a passive H^+ influx (or OH^- efflux).

As for the dependence of the passive H^+ influx on the external pH, it was reported (Bisson & Walker, 1980; Chilcott *et al.*, 1983; Smith & Walker, 1985) that the membrane permeability to H^+ increases at high pH.

As in the case of protons, HCO_3^- transport varies along the length of the cell. A comparison between the time courses of HCO_3^- and OH^- transport inactivation in response to two separately imposed dark treatments indicates that neighbouring transport regions respond in a highly correlated manner. This opens two possibilities (Lucas, 1982): either there exists H^+/HCO_3^- symport in Characean cells or extracellular CO_2 is produced in acidic regions and then diffuses into the cytoplasm. Lucas (1983) himself preferred the first alternative for the sake of simplicity.

An important role in the banding phenomenon is played by cyclosis. It was shown (Lucas & Dainty, 1977) that as a result of the inhibition of cyclosis by cytochalasin B the number of bands might increase up to 30–50 and their amplitude drastically decreases, or the bands completely disappear. The cytoplasmic motion was studied both experimentally and theoretically (Kamiya, 1986; Romanovsky & Chernjaeva, 1987). Cytoplasmic streaming has a self-sustained nature and is ensured by interaction of F-actin bundles bound to the chloroplast surface with myosin present in the endoplasmic matrix (Kamiya, 1986).

In our model we take into account the spatial distribution of H^+ and HCO_3^- ions inside and outside the cell as it results from their transport across the cell membrane. The scheme in Fig. 9 illustrates the processes relevant to the pattern formation.

The model is based on the following assumptions.

- The ion fluxes that determine patterns on the Characean cell membranes are those of H^+ and HCO_3^-.
- The H^+ efflux is due to a H^+ pump that transports protons against their electrochemical gradient.
- The H^+ influx occurs passively along an electrochemical gradient through channels, the permeability of which increases with the pH of the external medium.
- The H^+ pump is activated by ATP produced in the chloroplasts by photophosphorylation.

- Bicarbonate is utilized within the cell in the Calvin cycle and thus the rate of its utilization depends on the light intensity.
- We assume that bicarbonate ions are cotransported with protons into the cell.
- As the pH in the cell is buffered to a great extent (Walker & Smith, 1977; Savchenko *et al*., 2000), we take into account in the model only variations of H^+ concentration outside the cell. On the other hand, as we assume that bicarbonate in the external medium is in excess (Lucas & Nuccitelli, 1980), though not necessarily uniformly distributed, ¶we consider only interval variations of the HCO_3^- concentration.
- Bicarbonate inside the cell is transported both by diffusion and cyclosis (cytoplasmic motion). The latter may also influence the effective diffusion coefficient, resulting in a higher value.

In our phenomenological model we include these ion fluxes without accounting for the detailed mechanisms of the corresponding processes. The proton concentration h in the outer space is described by the diffusion equation

$$\frac{\partial h}{\partial t} = D_h \Delta h. \tag{1}$$

For the bicarbonate concentration c inside the cell the corresponding equation should contain, besides the diffusion term, a flow term due to cyclosis and also a term describing bicarbonate assimilation in photosynthetic processes

$$\frac{\partial c}{\partial t} = D_c \Delta c - dc - \mathbf{V} \cdot \nabla c. \tag{2}$$

Here $\mathbf{V}$ denotes the velocity of the cytoplasmic flow. In the term dc for the assimilation of bicarbonate, the value of d may vary as it is related to the local density of chloroplasts, which are non-uniformly distributed in space, occupying a thin layer near the inner surface of the cell membrane (Kamiya, 1986).

Equations (1) and (2) are solved for two separate regions, corresponding to the intercellular and external media, with a common boundary, which is the cell membrane. The sizes of these regions are $L \times H'$ and $L \times H$, respectively. The boundary conditions are zero fluxes on the outer boundaries, while on the common boundary the conditions are given by the following expressions:

$$\left.\frac{\partial h}{\partial y}\right|_{y=+0} = -\frac{1}{D_h} J_h, \quad \left.\frac{\partial c}{\partial y}\right|_{y=-0} = -\frac{1}{D_c} J_c. \tag{3}$$

The form of the flux terms J_h and J_c results from the specific processes taking place in the cell membrane. The proton flux consists of the efflux J_{ha} due to the H_+ pump and the passive influx J_{hp}. As the proton efflux is activated by ATP produced in photosynthesis, it should increase both with the bicarbonate concentration and the light intensity. The efficiency of the pump should decrease with the increase of the transmembrane electrochemical gradient. Thus J_{ha} may be expressed in the simplest form that meets these conditions

$$J_{ha} = \hat{I} \frac{c}{h + h_m}, \tag{4}$$

where $\hat{I}$ is a parameter monotonically growing with the light intensity. As the permeability of the membrane rises with pH, we take the proton influx in the form

$$J_{hp} = -\hat{p} \frac{h - h_0}{h^2}, \tag{5}$$

where h_0 is the intracellular proton concentration.

According to our assumptions, the bicarbonate flux is proportional to the proton influx:

$$J_c = -\hat{q} \frac{h - h_0}{h^2}. \tag{6}$$

Equations (1) and (2) with boundary conditions (3)–(6) are rather complicated for a direct

¶Though the outer H^+ concentration is connected to the HCO_3^- concentration and thus is not uniform, we suggest that these (variable) HCO_3^- concentrations are sufficient to ensure full rates of H^+/HCO_3^- symport in alkaline zones. It seems to be a reasonable assumption because at pH > pK (6.35) the CO_2–HCO_3^- equilibrium is shifted towards the HCO_3^- form.

analytical treatment. However, under certain conditions a reduction to a one-dimensional problem appears possible which is convenient for parametric analysis.

THE ONE-DIMENSIONAL MODEL

Let us integrate eqn (1) in the y-direction from 0 to H and eqn (2) from $-H'$ to 0 with the given boundary conditions. This yields

$$\frac{\partial \bar{h}}{\partial t} = \frac{1}{H}(J_{ha} + J_{hp}) + D_h \frac{\partial^2 \bar{h}}{\partial x^2},$$

$$\frac{\partial \bar{c}}{\partial t} = -\frac{1}{H'} J_c - d\bar{c} - V\frac{\partial \bar{c}}{\partial x} + D_c \frac{\partial^2 \bar{c}}{\partial x^2}, \qquad (7)$$

where $\bar{h}(x) = 1/H \int_0^H h\,\mathrm{d}y$ and $\bar{c}(x) = 1/H' \int_{-H'}^0 c\,\mathrm{d}y$.

The flux terms that enter eqn (7) are functions of h and c at $y = 0$, but not of the mean values $\bar{h}$ and $\bar{c}$ as are all the other terms. However, if the values of H and H' are small compared to the characteristic scale of the pattern, one can assume $h \approx \bar{h}$ and $c \approx \bar{c}$, which leads to

$$\frac{\partial h}{\partial t} = I\frac{c}{h + h_m} - p\frac{h - h_0}{h^2} + D_h \frac{\partial^2 h}{\partial x^2},$$

$$\frac{\partial c}{\partial t} = q\frac{h - h_0}{h^2} - dc - V\frac{\partial c}{\partial x} + D_c \frac{\partial^2 c}{\partial x}, \qquad (8)$$

where $I = \hat{I}/H$, $p = \hat{p}/H$ and $q = \hat{q}/H'$.

The uniform stationary state of eqns (8) (i.e. the point of intersection of the null-clines) is

$$h_s = \frac{qI}{pd} - h_m, \qquad c_s = \frac{q(h_s - h_0)}{dh_s^2}. \qquad (9)$$

In a linear approximation for the deviations $\bar{h} = h - h_s$ and $\bar{c} = c - c_s$ from the stationary state one obtains

$$\frac{\partial \bar{h}}{\partial t} = p\frac{h_s(h_m - h_0) - 2h_m h_0}{h_s^3(h_s + h_m)}\bar{h} + \frac{I}{h_s + h_m}\bar{c} + D_h \frac{\partial^2 \bar{h}}{\partial x^2}, \qquad (10)$$

$$\frac{\partial \bar{c}}{\partial t} = -q\frac{h_s - 2h_0}{h_s^3}\bar{h} - d\bar{c} - V\frac{\partial \bar{c}}{\partial x} + D_c \frac{\partial^2 \bar{c}}{\partial x^2}.$$

Linear stability analysis of eqns (10) shows that in the absence of diffusion and flow the stationary state is always stable. However, if

$$0 < p\frac{h_s(h_m - h_0) - 2h_m h_0}{h_s^3(h_s + h_m)} < d, \qquad (11)$$

then diffusion and/or flow may destabilize the uniform state. If $V = 0$ then instability is due to the Turing bifurcation, the conditions of which are obtained in a standard way (see, for example, Murray, 1989 and Nicolis & Prigogine, 1977). The results of the corresponding analysis, shown in Fig. 10, demonstrate that for the Turing bifurcation a sufficiently high ratio of the diffusion coefficients D_c/D_h is essential. Namely, for the parameters used in simulations it should be greater than two (see Fig. 10). Meanwhile, as shown in the appendix, differential flow may destabilize the uniform distribution, even if the conditions of the Turing bifurcation are not met

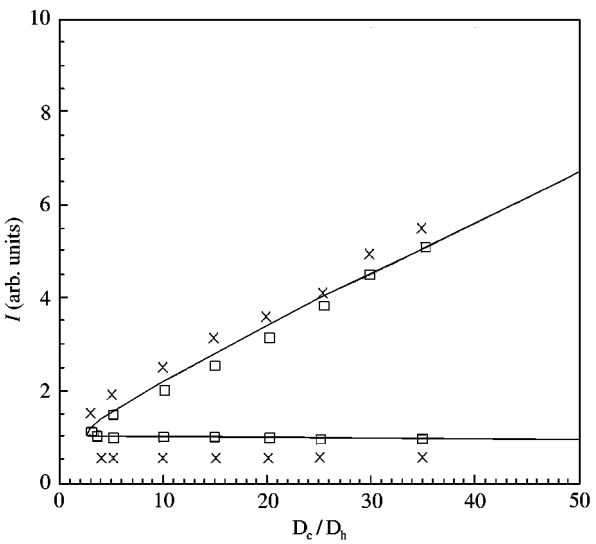

FIG. 10. Cross-section of the parametric space of eqns (8) in the plane (I, D_c/D_h) obtained by linear stability analysis (all other parameters are fixed and equal to those used in simulations). The solid line separates the region of stability of the homogeneous stationary state (outside) from the region, in which the homogeneous state is unstable (inside). Crosses and squares correspond to the results of numerical simulations. Crosses indicate the cases when no pattern arises, squares are for those cases when patterns are formed.

(see also Rovinsky & Mezinger, 1992 and Lobanov *et al.*, 2000).

Thus, returning to the object under consideration, we point out that cyclosis in *Chara* cells could be important for pattern formation, as it both increases the effective diffusion coefficient of bicarbonate, creating conditions for the Turing bifurcation, and produces differential flow.

In the following, we give the results of numerical simulations for both the reduced one-dimensional model and the original two-dimensional model.

NUMERICAL SIMULATIONS FOR THE ONE-DIMENSIONAL MODEL

In the first series of computations, we investigate the behaviour of the model for different values of parameters associated with the light intensity and the diffusion of the components. At this stage, we disregard differential flow and assume that cyclosis increases the effective diffusion coefficient of c (bicarbonate inside the cell). The parameters used in all the simulations are $h_m = 10$, $h_0 = 0.25$, $q = 1050$, $p = 10$, $d = 10$ and $D_h = 1$. Simulations were performed in an interval containing 240 points with zero-flux boundary conditions; the explicit numerical scheme was used. For initial conditions small spatial perturbations near the homogeneous state were applied.

Figure 11 depicts stationary patterns formed for different values of the diffusion coefficient D_c and the parameter I associated with the light intensity. In order to be able to compare simulation results with the observed pH profiles the value of lgh is shown. One can see that the spatial scale of the pattern decreases with the increase of the "light intensity" I, which agrees well with the experimental observations. If I is less than a certain threshold value, the pattern disappears; thus, the model reproduces the observed threshold dependence of the banding pattern on the light intensity. Figure 12 represents the results of

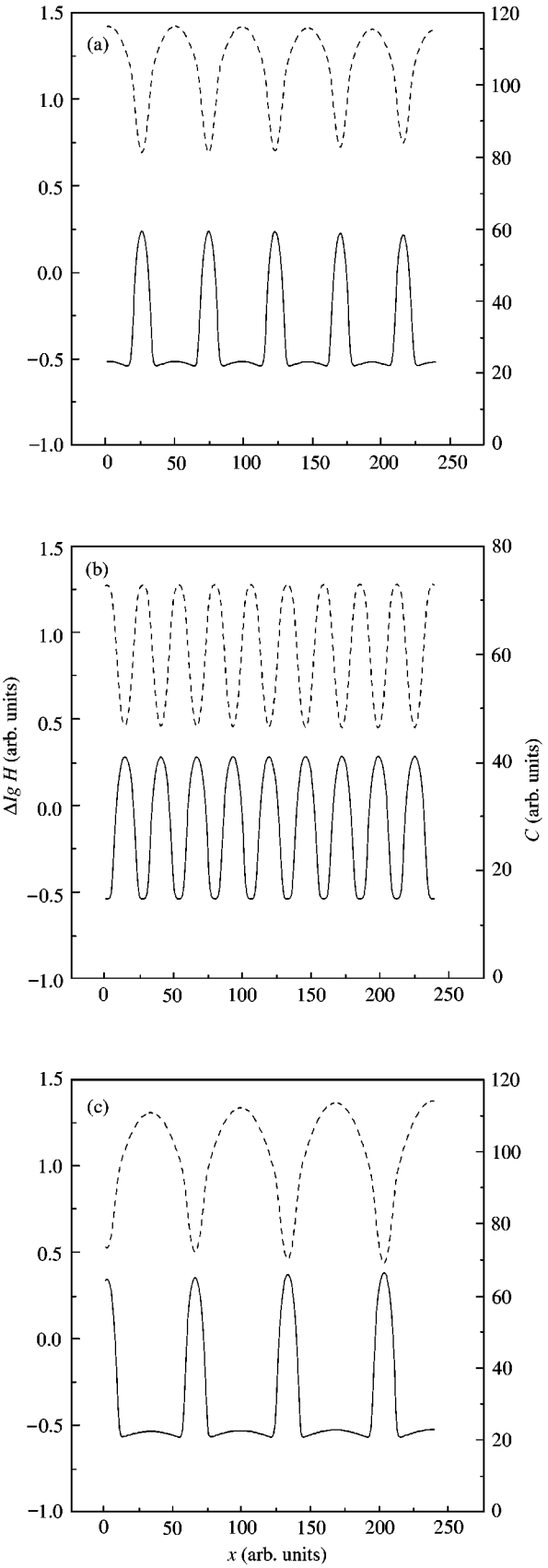

FIG. 11. Spatial distributions of the deviation of the logarithm of the variable h (solid line) and of the variable c (dotted line) obtained numerically for the one-dimensional model (8). The parameters used in simulations: $h_m = 10$, $h_0 = 0.25$, $q = 1050$, $p = 10$, $d = 10$, $D_h = 1$; (a) $I = 1.0$, $D_c = 10$; (b) $I = 1.5$, $D_c = 10$; (c) $I = 1.0$, $D_c = 15$.

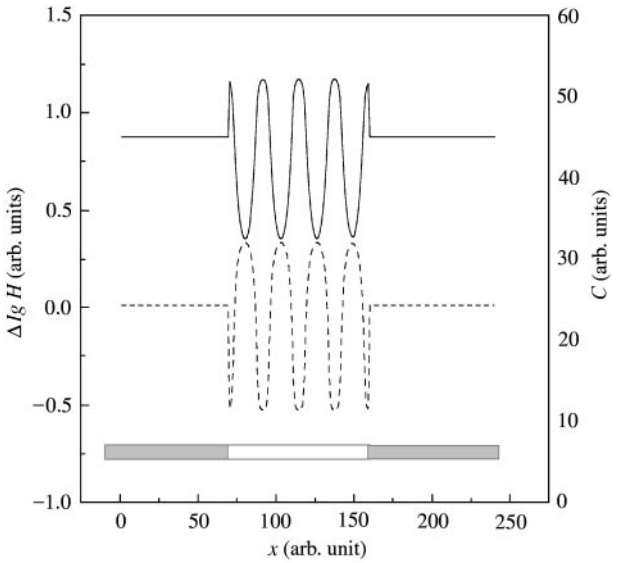

FIG. 12. Spatial distributions of the deviation of the logarithm of the variable h (solid line) and of the variable c (dotted line) in the case when the parameter I is not spatially uniform: in the outer regions $I = 0.75$ while in the middle $I = 1.2$.

simulations for the case when only a part of the cell is illuminated. The pattern forms only in the region of illumination as is observed in experiments (cf. Fig. 6).

In order to verify numerically the results of the parametric analysis of the model, a series of simulations was performed for different values of the parameters I and D_c. Each simulation corresponds to a point in the plane of Fig. 10. Crosses indicate the cases when no pattern arises, squares are for those cases when patterns are formed. Simulations completely confirmed the results of analytical treatment.

NUMERICAL SIMULATIONS FOR THE TWO-DIMENSIONAL MODEL

In the second series of computations, the behaviour of the basic two-dimensional model was investigated. Simulations were performed for two rectangular domains with a common boundary: 240×30 points for the variable h and 240×10 for the variable c. Chloroplasts, in which bicarbonate is assimilated, are located in a thin layer near the plasmalemma. Thus, one can either assume that the parameter d in eqn (2) is non-zero only in a few rows of the grid near the boundary, or one formally considers that this layer belongs to the boundary, thus excluding the corresponding term from eqn (2) and including it in the boundary condition. Both approaches give similar results. In our simulations we used the second of them.

Figure 13 shows the profiles of concentrations of h and c in near-membrane layers obtained in simulations of the two-dimensional model for different values of the parameters I and D_c. All other parameters are the same as the corresponding parameters in the one-dimensional model. The dependence on the parameters and shapes of the curves in one- and two-dimensional models appear to be very much alike (cf. Figs 11 and 13). The only difference is that the spatial scale of the two-dimensional pattern is smaller for the same parameters than that of the one-dimensional pattern. This is not surprising, because the transition from the two-dimensional to the one-dimensional model leads to a re-scaling of the parameters that enter the flux terms (see above). Thus, as does the one-dimensional model, the two-dimensional model qualitatively explains a large variety of effects observed in our experiments for different regimes of illumination which were described above.

Finally, Fig. 14 represents a set of two-dimensional distributions of the proton concentration obtained numerically for successive instants of time. The light patches correspond to higher proton concentration. Initially, many bands start to form, but in the course of time only a few of them survive. A quite similar behaviour was indeed observed in *Chara* cell when a banding pattern is formed (cf. Fig. 5).

Discussion

A newly developed experimental method, based on the application of antimony pH microelectrodes, appears to be a very convenient and powerful tool for studying acid and alkaline band formation in Characean cells. Unlike the vibrating probe techniques the antimony electrode practically does not perturb the concentration gradients thus increasing the accuracy of the measurements. As a further advantage, the electrode moving along the cell continuously scans the whole profile of pH values. Thus, beyond reproducing the experimental data obtained

earlier by other investigators, new essential features of the phenomenon were discovered such as, for instance, unclosed bands.

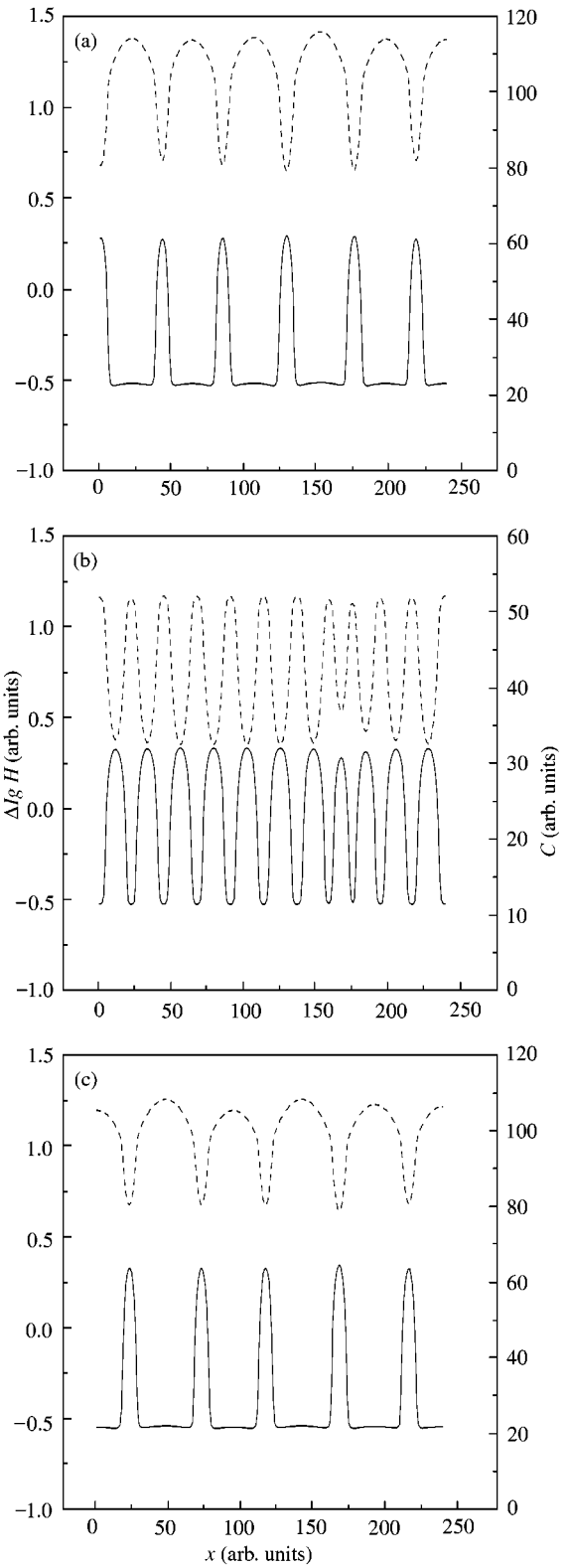

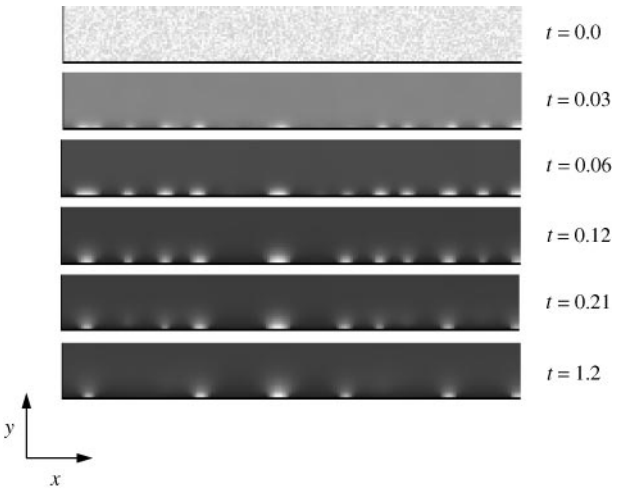

FIG. 14. The dynamics of pattern formation in the two-dimensional model. The initial four transient and the final spatial proton distributions are shown. The parameters used in simulations: $h_m = 10$, $h_0 = 0.25$, $q = 1050$, $p = 10$, $d = 10$, $D_h = 1$, $I = 1.0$, $D_c = 12$.

It is well known that acid and alkaline bands are formed on a membrane of a *Chara* cell only if the latter is illuminated with sufficiently strong light intensity. We have investigated the dependence of the amplitude of the pattern and its spatial scale on light intensity. It turns out that the amplitude does not gradually change with the latter, as could be expected, but that a threshold phenomenon is involved in that it practically remains constant in a very broad range of light intensity (about two orders of magnitude) but then abruptly disappears below a critical intensity level.

As for the relationship between the spatial scale of the pattern and the light intensity, it essentially depends on the initial conditions. If the cell was initially well illuminated and then the light intensity was decreased to the value which is higher than the threshold, the final pattern remained practically the same as the initial one and the spatial scale also did not change. However, if initially the cell was in darkness and then was

FIG. 13. Spatial distributions of the deviation of the logarithm of the variable h (solid line) and of the variable c (dotted line) in the premembrane layers obtained numerically for the two-dimensional model (1)–(3). The parameters used in simulations: $h_m = 10$, $h_0 = 0.25$, $q = 1050$, $p = 10$, $d = 10$, $D_h = 1$; (a) $I = 1.0$, $D_c = 15$; (*b*) $I = 2.0$, $D_c = 15$; (c) $I = 1.0$, $D_c = 10$.

exposed to light, the characteristic period of the pattern became smaller with increasing light intensity. The number and position of bands, constant under stationary light regime, may increase or decrease upon the abrupt changes in light intensity. Thus, these bands are unlikely to be associated with static morphological structures. It seems more likely that band formation represents a self-organization phenomenon.

Dynamic characteristics of the process of pattern formation were also investigated. The time of both disappearance and recovery of the pattern, as a result of switching the light off and on, was about tens of minutes or at most an hour. The question arises as to why the alkaline peaks come back practically at the same positions after re-illumination of the cell. In our view, this could be due to the occurrence of long-lived residual phenomena in cells transferred from light to darkness. It is conceivable that manifestations of banding phenomena are not restricted to changes in ion and gas composition of the external medium. Low-amplitude long-lived changes in the internal compartments (cytoplasm, chloroplasts) may play a role similar to that of nucleation centres in crystallization. Even if these inhomogeneities are not readily detected, they might facilitate the band formation at the same positions upon re-illumination.

New results were obtained in experiments when pH profiles were scanned on different paths along the cell and also in transversal direction. It should be clear that the peculiar shapes of transversal profiles (profiles with maxima) observed in both acid and alkaline regions, are related to the lack of complete circumferential symmetry in the distribution of H^+-exporting and H^+-consuming domains on the surface of *Chara* cells. Thus, the complicated shapes of transversal pH profiles are due to the presence of unclosed pH bands or strips, rather than the consequence of spatially restricted diffusion in narrow grooves.

On the whole, the phenomenology of the acid and alkaline patterns strongly supports the idea that in fact they are dynamic self-organizing structures (Toko *et al*., 1985). These structures have a number of general properties (see, for example, Nicolis & Prigogine, 1977), which were successfully described by previous models (Toko *et al*., 1985, 1987a; Leonetti & Pelce, 1994). The phenomenological model presented here is based on a number of assumptions that have direct experimental support. At this stage, our goal was to demonstrate that the principles that form the basis of the model are in accordance with the observed phenomena. In fact, the model correctly describes the dependence of the pattern characteristics on the light intensity. It demonstrates the threshold dependence of the pattern on the level of illumination as observed in the *Chara* cell. The number of bands of the stationary pattern obtained in computations increases with the light intensity in agreement with the experimental data. The dynamics of the patterns arising from a uniform state is also well reproduced in the numerical simulations.

One of the obvious differences of the experimental data and calculations is that the experimental patterns are semi-regular while the calculated ones are fairly regular. This can be easily explained by the natural inhomogeneity of a living cell while in the model everything is assumed to be uniform.

The model reveals the role of cyclosis in banding patterns. Cyclosis both increases the effective diffusion of bicarbonate inside the cell and creates differential flow. As is shown analytically and in simulations, both effects can lead to instability of the homogeneous state and thus to pattern formation.

In the present schematic form, the model does not pretend to explain in full the variety of the results obtained in experiments. For instance, the effect of chemical agents on the pH pattern calls for a more detailed description of the system. However, even in this form the model provides a key to an explanation. The model parameters h_0 corresponds to the internal proton concentration, which essentially determines the pattern. On the other hand, weak acids and bases, as mentioned above, should influence the internal pH level. Thus, the effect of chemical agents can be interpreted as a variation of the parameter h_0.

So far, we did not discuss in this framework the unclosed bands observed in experiments as it is an essentially three-dimensional effect.

The model has a large potential for further development. In the present form, it is just a skeleton which will further be filled with details of the intimate processes taking place in the cell.

Especially, the role of the photosynthetic system in pattern formation and molecular mechanisms of ion transport across the membrane should be incorporated into the model.

Support by grants from the Deutsche Forschungsgemeinschaft and the Russian Foundation of Basic Research is gratefully acknowledged.

REFERENCES

ANTONENKO, YU, N. & BULYCHEV A. A. (1991). Measurements of local pH changes near bilayer lipid membrane by means of a pH microelectrode and a protonophjore-dependent membrane potential. Comparison of the methods. *Biochim. Biophys. Acta* **1070,** 279–282.

ARENS, K. (1939). Physiologische Multipolarit der Zelle von *Nitella* whrend der Photosynthese. *Protoplasma* **33,** 295–311.

BISSON, M. A. & WALKER, N. A. (1980). The *Chara* plasmalemma at high pH. Electrical measurements show rapid specific passive uniport of H^+ or OH^-. *J. Mem. Biol.* **56,** 1–7.

BUDRENE, E. O. & BERG, H. C. (1991). Complex patterns formed by motile cells of *Escherichia coli*. *Nature* **349,** 630–633.

CHILCOTT, T. C., COSTER, H. G. L., OGATA, K. & SMITH, J. R. (1983). Spatial variation of the electrical properties of *Chara australis*. II. Membrane capacitance and conductance as a function of frequency. *Aust. J. Plant Physiol.* **10,** 352–362.

DEVREOTES, P. N. (1989). *Dictyostelium discoideum*: a model system for cell–cell interactions in development. *Science* **245,** 1054–1058.

DORN, A. & WEISENEEL, M. H. (1984). Growth and the current pattern around internodal cells of *Nitella flexilis* L. *J. Exp. Bot.* **35,** 373–383.

ELZENGA, J. T. M. & PRINS, H. B. A. (1989). Light-induced polar pH changes in leaves of *Elodea canadensis*. *Plant Physiol.* **91,** 62–67.

FISAHN, J. & LUCAS, W. J. (1992). Direct measurement of the reversal potential and current–voltage characteristics in the acid and alkaline regions of *Chara coralina*. *Planta* **186,** 241–248.

FISAHN, J. & LUCAS, W. J. (1995). Spatial organization of transport domains and subdomain formation in the plasma membrane of *Chara corallina*. *J. Mem. Biol.* **147,** 275–381.

FROMHERZ, P. (1998a). Spatio-temporal patterns in the fluid-mosaic model of membranes. *BBA* **944,** 108–111.

FROMHERZ, P. (1998b). Self-organization of the fluid mosaic of charged channel proteins in membranes. *Proc. Natl Acad. Sci. U.S.A.* **85,** 6353–6357.

IWABUCHI, A., YANO, M. & SHIMIZU, H. (1989). Development of extracellular electric pattern around lepidium roots: its possible role in root growth and gravitropism. *Protoplasma* **148,** 94–100.

JAFFE, L. F. (1977). Electrophoresis along cell membranes. *Nature* **265,** 600–602.

JAFFE, L. F., ROBONSON, K. R. & NUCCITELLI, R. (1974). Local cation entry and self-electrophoresis as an intracellular localization mechanism. *Ann. N. Y. Acad. Sci.* **238,** 372.

KONDO, S. & ASAI, R. (1995). Turing patterns in fish skin? *Nature* **376,** 765–768.

LARTER, R. & ORTOLEVA, P. (1982). A study of instability to electrical symmetry breaking in unicellular system. *J. theor. Biol.* **96,** 175–200.

LEONETTI, M. & PELCE, P. (1994). On the theory of the pH bands in characean algae. *C. R. Acad. Sci. Paris, Sciences de la vie/Life Sci.* **317,** 801–805.

LOBANOV, A. I., PLUSNINA, T. YU., RIZNICHENKO, G. YU., STAROZHILOVA, T. K. & RUBIN, A. B. (2000). Influence of electric field on patterns in a reaction–diffusion system. *Biofizika* **45,** 495–502 (in Russian).

LUCAS, W. J. (1975). Photosynthetic fixation of carbon by internodal cells of *Chara corallina*. *J. Exp. Bot.* **26,** 331–346.

LUCAS, W. J. (1976). Plasmalemma transport HCO_3^- and OH^- in *Chara corallina*: non-antiporter systems. *J. Exp. Bot.* **27,** 19–31.

LUCAS, W. J. (1979). Alkaline band formation in *Chara corallina*: due to OH^--efflux or H^+-influx? *Plant Physiol.* **63,** 248–254.

LUCAS, W. J. (1982). Mechanism of acquisition of exogenous bicarbonate by internodal cells of *Chara corallina*. *Planta* **156,** 181–192.

LUCAS, W. J. (1983). Photosynthetic assimilation of exogenous HCO_3^- by aquatic plants. *Ann. Evol. Plant Physiol.* **34,** 71–104.

LUCAS, W. J. & DAINTY, J. (1977). Spatial distribution of functional OH^- carriers along a Characean internodal cell: determined by the effect of cytochalasin B on HCO_3^- Assimilation *J. Mem. Biol.* **32,** 75–92.

LUCAS, W. J. & NUCCITELLI, R. (1980). HCO_3^- and OH^- transport across the plasmalemma of *Chara*. *Planta* **150,** 120–131.

MARRE, E. (1979). Fusicoccin: a tool in plant physiology. *Annu. Rev. Plant Physiol.* **30,** 273–288.

MEINHARDT, H. (1982). *Models of Biological Pattern Formation*. New York: Academic Press.

METRAUX, J. P., RICHMOND, P. A. & TAIZ, L. (1980). Control of cell elongation in *Nitella* by endogeneous cell wall pH gradients. Multiaxial extensibility and growth studies. *Plant Physiol.* **65,** 204–210.

MÜLLER, S. C. & PLESSER, Th. (1992). *Spato-Temporal Organization in Nonequilibrium Systems*. Dortmund: Project-Verlag.

MURRAY, J. D. (1989). *Mathematical Biology*. Berlin: Springer-Verlag.

NICOLIS, G. & PRIGOGINE, I. (1977). *Self-Organization in Nonequilibrium Systems*. New York: Wiley.

OGATA, K. (1983). The water-film electrode: a new device for measuring the characean electro-potential and conductance distributions along the length of the internode. *Plant Cell Physiol.* **24,** 695–703.

POLEZHAEV, A. A. & SABUROV, R. A. (1991). Model of spatial pattern formation by ionic channels on a cell membrane surface. *Biofizika* **36,** 805–809 (in Russian).

REID, R. J., SMITH, F. A., SODEN, A. & TURNBUL, A. R. (1989). Regulation of metabolism by intracellular pH: Inhibition of photosynthesis by weak acids in intact cells of *Chara corallina*. *Plant Sci.* **65,** 15–23.

REMIS, D., BULYCHEV, A. A. & KURELLA, G. A. (1986). The electrical and chemical components of the protonmotive force in chloroplast as measured with capillary and pH-sensitive microelectrodes. *Biochim. Biophys. Acta* **852,** 68–73.

ROMANOVSKY, YU. M. & CHERNJAEVA, E. B. (1987). Hydrodynamics of intercellular cytoplasm flows. In: *Thermodynamics of Irreversible Processes* (Lopushansky, A. I., ed.), pp. 152–162. Moscow: Nauka.

ROVINSKY, A. B. & MENZINGER, M. (1992). Chemical instability induced by a differential flow. *Phys. Rev. Lett.* **69,** 1193–1196.

SAVCHENKO, G., WIESE, C., NEIMANIS, S., HEDRICH, R. & HEBER, U. (2000). pH regulation in apoplastic and cytoplasmic cell compartments of leaves. *Planta* **211,** 246–255.

SIEGERT, F. & WEIJER, C. J. (1993). The role of periodic signals in the morphogenesis of *Dictyostelium discoideum*. In: *Oscillations and Morphogenesis* (Rensing, L., ed.), pp. 133–152. New York: Marcel Dekker.

SMITH, F. A. (1980). Comparison of the effects of ammonia and methylamine on chloride transport and intracellular pH in *Chara corallina*. *J. Exp. Bot.* **31,** 597–606.

SMITH, J. R. & WALKER, N. A. (1983). Membrane conductance of *Chara* measured in acid and basic zones. *J. Mem. Biol.* **73,** 193–202.

SMITH, J. R. & WALKER, N. A. (1985). Effects of pH and light on the membrane conductance measured in the acid and basic zones of *Chara*. *J. Mem. Biol.* **83,** 193–205.

SPEAR, D. G., BARR, J. K. & BARR, C. E. (1969). Localization of hydrogen ion and chloride fluxes in *Nitella*. *J. Gen. Physiol.* **54,** 397–414.

TOKO, K., CHOSA, H. & YAMAFUJI, K. (1985). Dissipative structure in the Characeae: Spatial pattern of proton flux as a dissipative structure in characean cells. *J. theor. Biol.* **114,** 127–175.

TOKO, K., FIJIYOSHI, T., OGATA, K., CHOSA, H. & YAMAFUJI, K. (1987a). Theory of electric dissipative structure in Characean internode. *Biophys. Chem.* **27,** 149–172.

TOKO, K., IIYAMA, S., TANAKA, C., HAYASHI, K., YAMAFUJI, K. & YAMAFUJI, K. (1987b). Relation of growth to spatial patterns of electric potential and enzyme activity in bean roots. *Biophys. Chem.* **27,** 39–58.

TOKO, K., HAYASHI, K., YOSHIDA, T., FUJIYOSHI, T. & YAMAFUJI, K. (1988). Oscillations of electric spatial patterns emerging from the homogeneous state in characean cells. *Eur. Biophys. J.* **16,** 11–21.

TURING, A. M. (1952) The chemical basis of morphogenesis. *Philos. Trans. R. Soc. Lond. B. Biol. Sci.* **237,** 37–72.

WALKER, N. A. & SMITH, F. A. (1977). Circulating electric current between acid and alkaline zones associated with HCO_3^- assimilation in *Chara*. *J. Exp. Bot.* **28,** 1190–1206.

WALKER, N. A., BEILBY, M. J. & SMITH, F. A. (1979). Amine uniport at the plasmalemma of charophyte cells: I. Current–voltage curves, saturation kinetics, and effects of unstirred layers. *J. Mem. Biol.* **49,** 21–55.

APPENDIX

The conditions for the Turing instability in reaction–diffusion systems are well known (see, for example, Murray, 1989). Here we obtain conditions for the instability of the uniform state for the more general case when an additional flow term is present in one of the equations. Let us consider a set of linear equations:

$$\frac{\partial u}{\partial t} = a_{11}u + a_{12}v + \frac{\partial^2 u}{\partial x^2},$$
$$\frac{\partial v}{\partial t} = a_{21}u + a_{22}v - E\frac{\partial v}{\partial x} + D\frac{\partial^2 c}{\partial x^2}. \tag{A.1}$$

Assume that without diffusion and flow the stationary state $u = v = 0$ is stable:

$$a_{11} + a_{22} < 0, \tag{A.2}$$

$$a_{11}a_{22} - a_{12}a_{21} > 0. \tag{A.3}$$

Substituting u and v into the set (A.1) in the form $u, v \sim \exp(\lambda t + \mathrm{i}kr)$ we obtain the following dispersion equation:

$$(\lambda + k^2 - a_{11})(\lambda + Dk^2 - a_{22} + \mathrm{i}Ek) - a_{12}a_{21} = 0. \tag{A.4}$$

It can be rewritten in the form

$$\lambda^2 - 2\lambda(A - \mathrm{i}\varphi) + A^2 - B^2 - a_{12}a_{21} - 2\mathrm{i}(A + B)\varphi = 0, \tag{A.5}$$

where $A = (a_{11} + a_{22} - (D + 1)k^2)/2$, $B = (a_{11} - a_{22} + (D - 1)k^2)/2$ and $\varphi = Ek/2$.

Note that the conditions of the Turing instability in the case $\varphi = 0$ (no flow) follow from the requirement that the roots of eqn (A.5) are real and have opposite signs: $A^2 - B^2 - a_{12}a_{21} < 0$. In the general case the roots of this equation are

$$\lambda_{1,2} = A \pm \sqrt{\frac{\sqrt{(B^2 - \varphi^2 + a_{12}a_{21})^2 + 4B^2\varphi^2} + B^2 - \varphi^2 + a_{12}a_{21}}{2}} + \mathrm{i}\left(-\varphi \pm \sqrt{\frac{\sqrt{(B^2 - \varphi^2 + a_{12}a_{21})^2 + 4B^2\varphi^2} - B^2 + \varphi^2 - a_{12}a_{21}}{2}}\right). \tag{A.6}$$

In view of condition (A.2) $A < 0$ for any k. Thus, the uniform stationary state becomes

unstable if one of the roots in eqn (A.6) has a positive real part

$$\Re\lambda_1 = A + \frac{\sqrt{\sqrt{(B^2 - \varphi^2 + a_{12}a_{21})^2 + 4B^2\varphi^2} + B^2 - \varphi^2 + a_{12}a_{21}}}{2} > 0 \tag{A.7}$$

This condition can be transformed to the form

$$A^2(B^2 - A^2 + a_{12}a_{21}) + \varphi^2(B^2 - A^2) > 0. \tag{A.8}$$

If $\varphi = 0$, condition (A.8) is reduced to the condition of the Turing instability: $B^2 - A^2 + a_{12}a_{21} > 0$. For $B^2 - A^2 + a_{12}a_{21} < 0$, condition (A.8) can still be met for sufficiently large φ^2, i.e. for sufficiently fast flow, if for some k

$$(B^2 - A^2) > 0. \tag{A.9}$$

The latter is possible only if

$$a_{11}a_{22} < 0. \tag{A.10}$$

Thus, if conditions (A.2), (A.3) and (A.10) are met [for our model, conditions (A.2) and (A.10) are equivalent to the single condition (11)], the uniform stationary state can be destabilized by a differential flow for any values of the diffusion coefficients.